Science Advances
AAAS

Supplementary Materials for

Symmetry disruption commits vault particles to disassembly

Pablo Guerra, María González-Alamos, Aida Llauró, Arnau Casañas, Jordi Querol-Audí, Pedro J. de Pablo, Núria Verdaguer*

*Corresponding author. Email: nvmcri@ibmb.csic.es

Published 9 February 2022, *Sci. Adv.* **8**, eabj7795 (2022)
DOI: 10.1126/sciadv.abj7795

This PDF file includes:

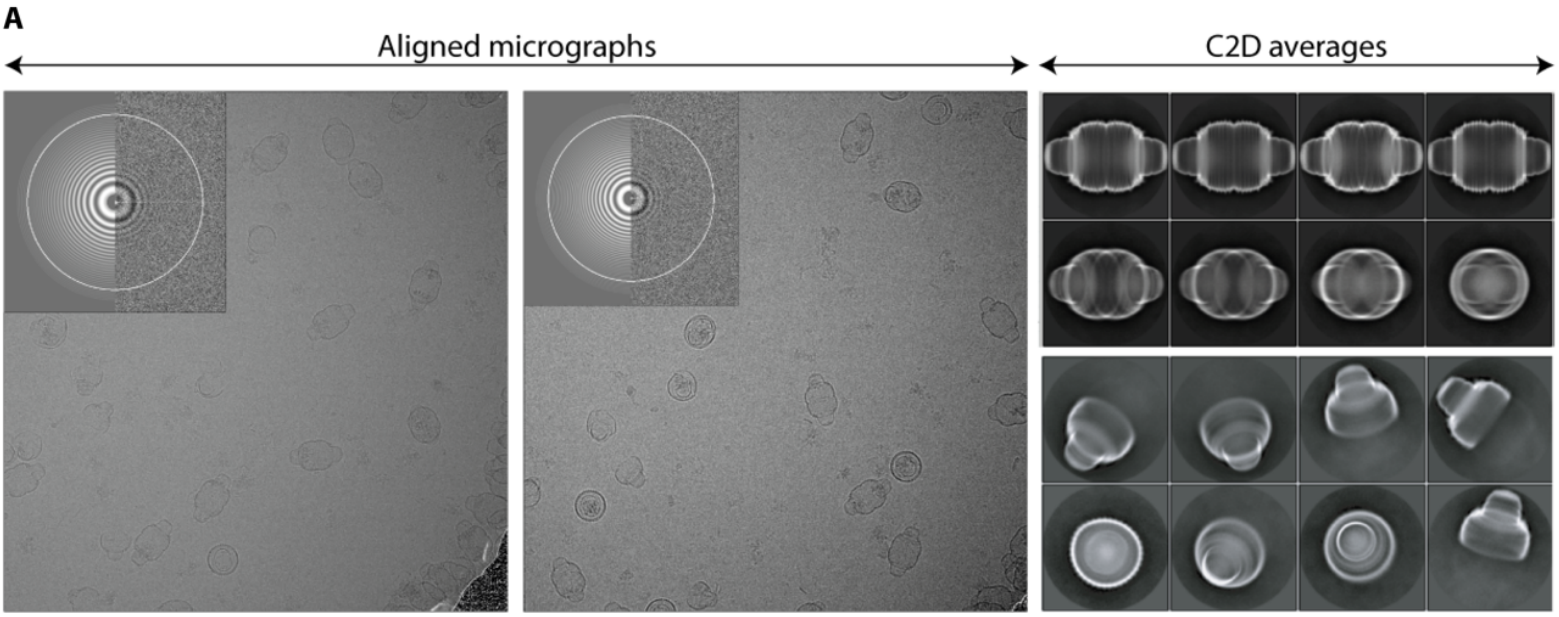
A
Aligned micrographs
C2D averages

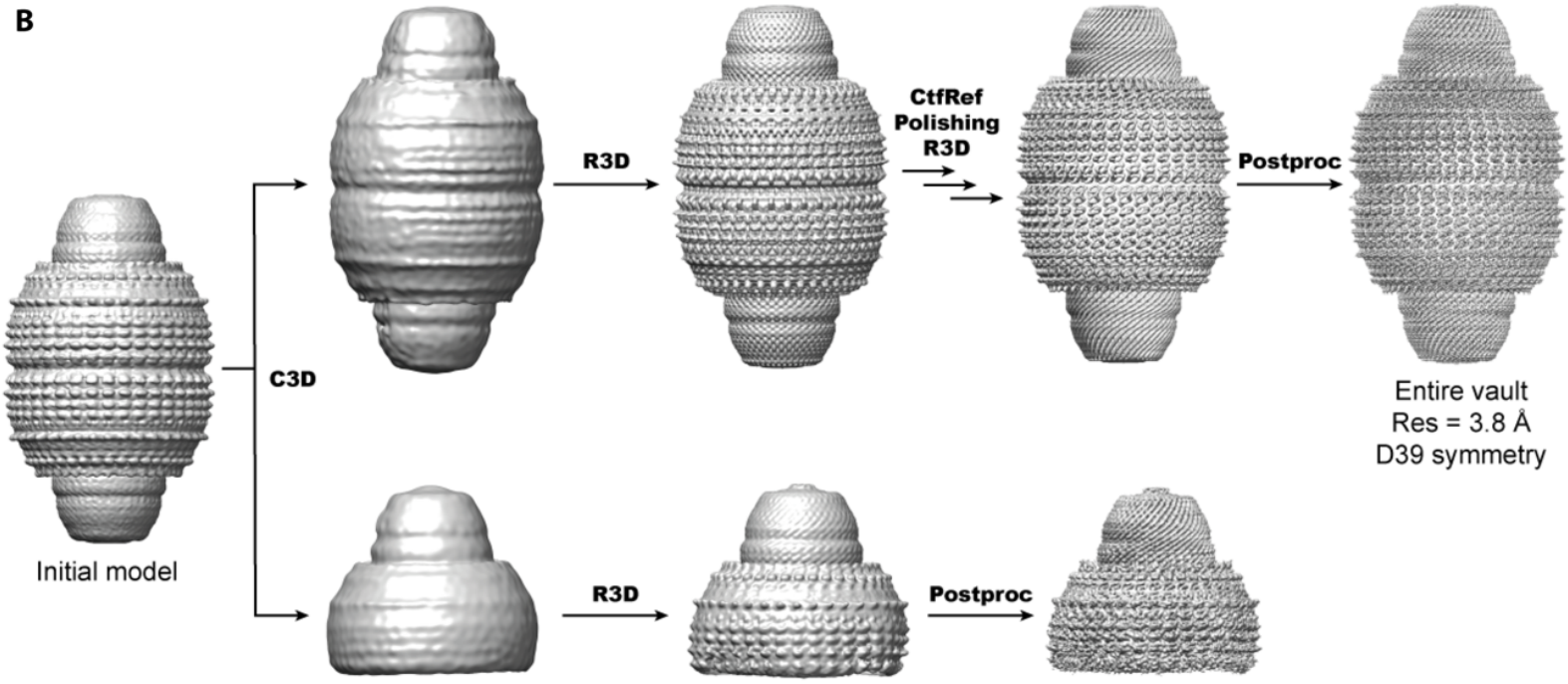
B
Initial model
C3D
R3D
R3D
CtfRef
Polishing
R3D
Postproc
Postproc
Entire vault
Res = 3.8 Å
D39 symmetry
Half-vault
Res = 7.0 Å
C1 symmetry

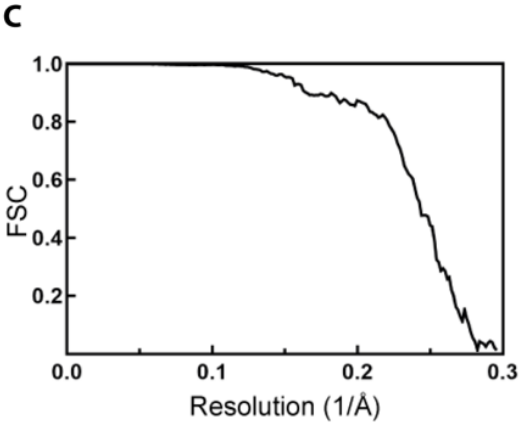
C
FSC
1.0
0.8
0.6
0.4
0.2
0.0
0.1
0.2
0.3
Resolution (1/Å)

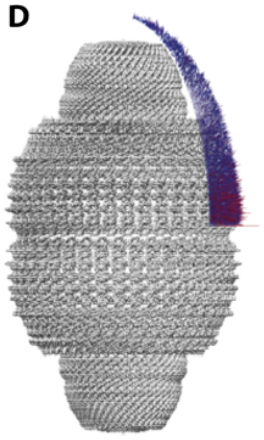
D

Figure S1. Cryo-EM representative images, classification workflow, FSC correlation curve and angular distribution for the symmetrical vault class. (**A**) Left, two representative aligned micrographs. Right, representative reference-free two-dimensional class averages (**B**) Image processing workflow used to characterize the heterogenous dataset what allowed the identification of several populations. (**C**) Gold-standard Fourier Shell Correlation (FSC) curves between half-maps refined independently using Relion 3. Global resolution by the 0.143 cutoff criterium was estimated to be 3.7 Å. (**D**) Angular distribution of vault particles that contributed to the final map.

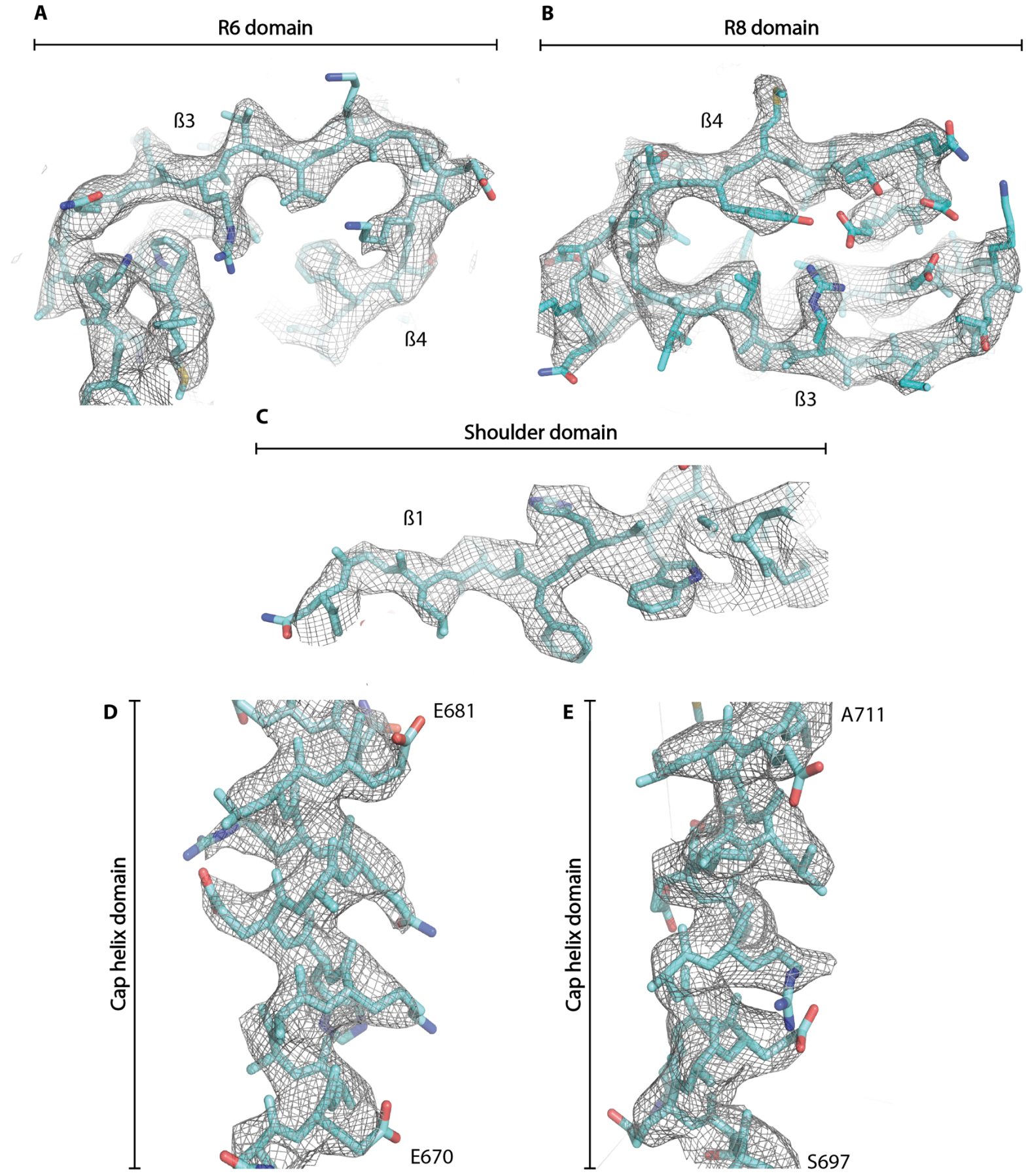
A
R6 domain
ß3
ß4
B
R8 domain
ß4
ß3
C
Shoulder domain
ß1
D
Cap helix domain
E681
E670
E
Cap helix domain
A711
S697

Figure S2. Experimental cryo-EM density for selected regions of the symmetrical vault reconstruction. (**A**) Experimental cryo-EM density observed for the ß3 motif of the R6 domain. (**B**) Cryo-EM density observed for the ß3 and ß4 motifs of the R8 domain. (**C**) Cryo-EM density observed for the ß1 motif of the shoulder domain. (**D** and **E**) Cryo-EM density observed in the cap helix domain.

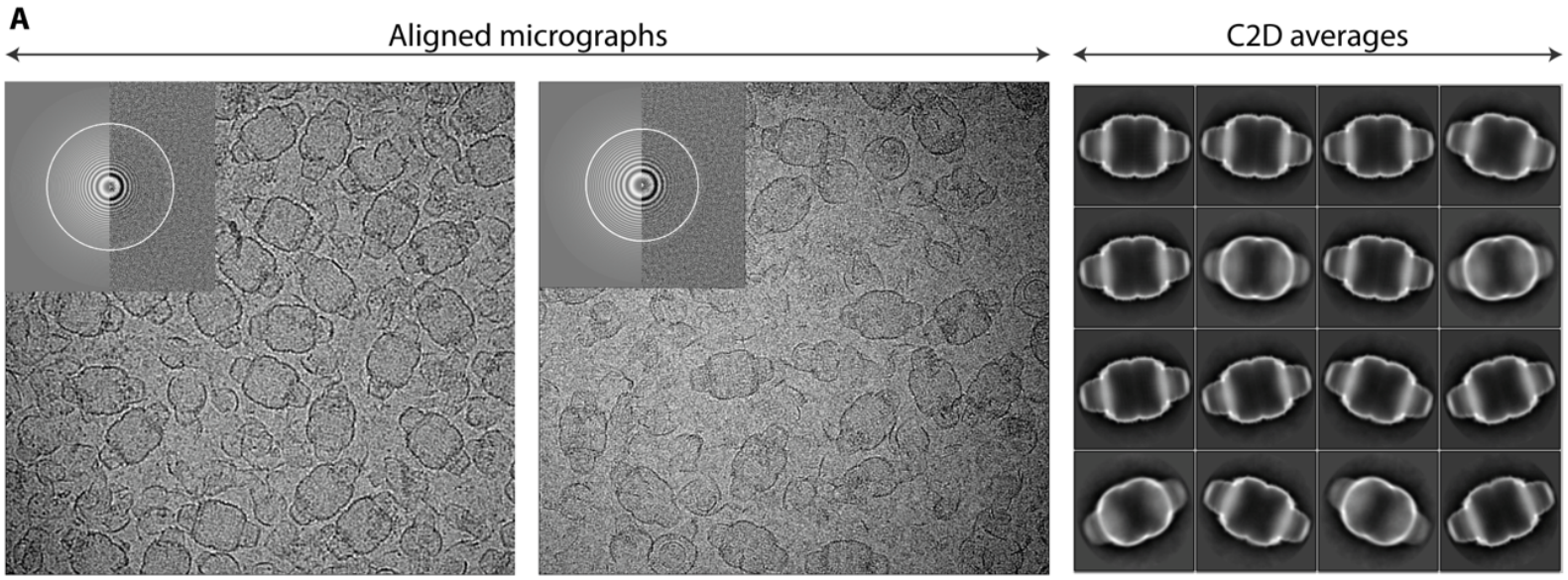
A
Aligned micrographs
C2D averages

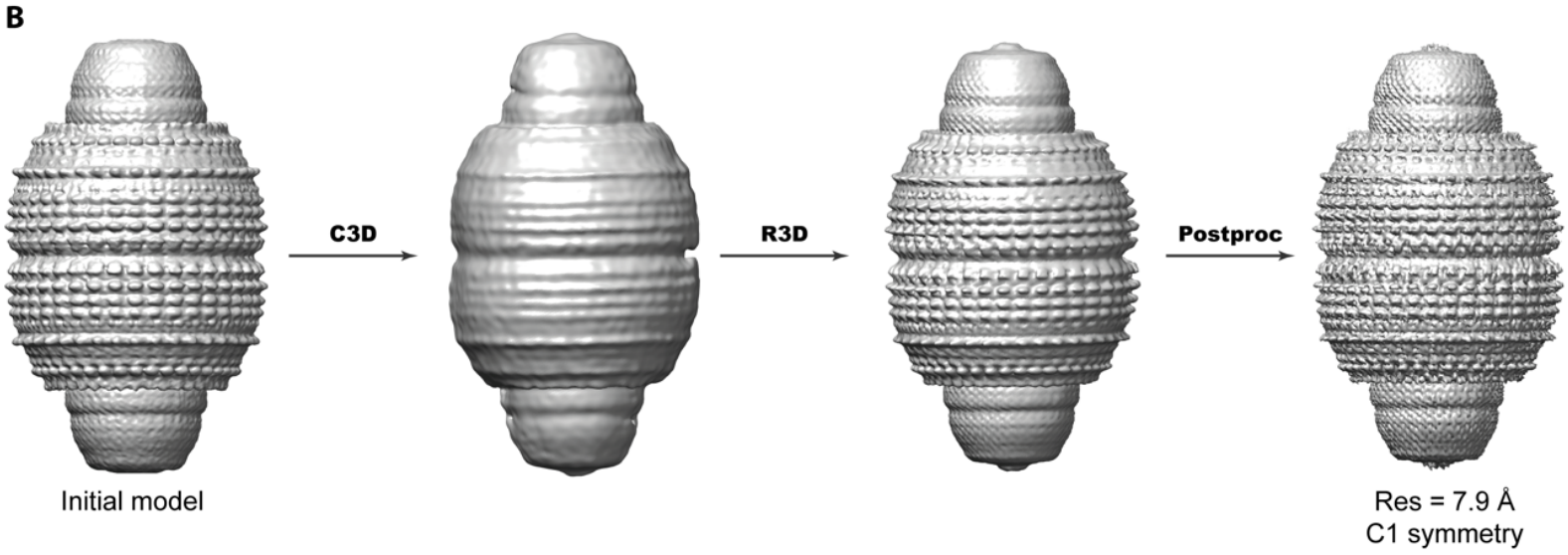
B
C3D
R3D
Postproc
Initial model
Res = 7.9 Å
C1 symmetry

Figure S3. Cryo-EM representative images and classification workflow for the asymmetrical vault class. (**A**) Left, two representative aligned micrographs. Right, representative reference-free two-dimensional class averages. (**B**) Image processing workflow used to identify the open committed vault conformation.

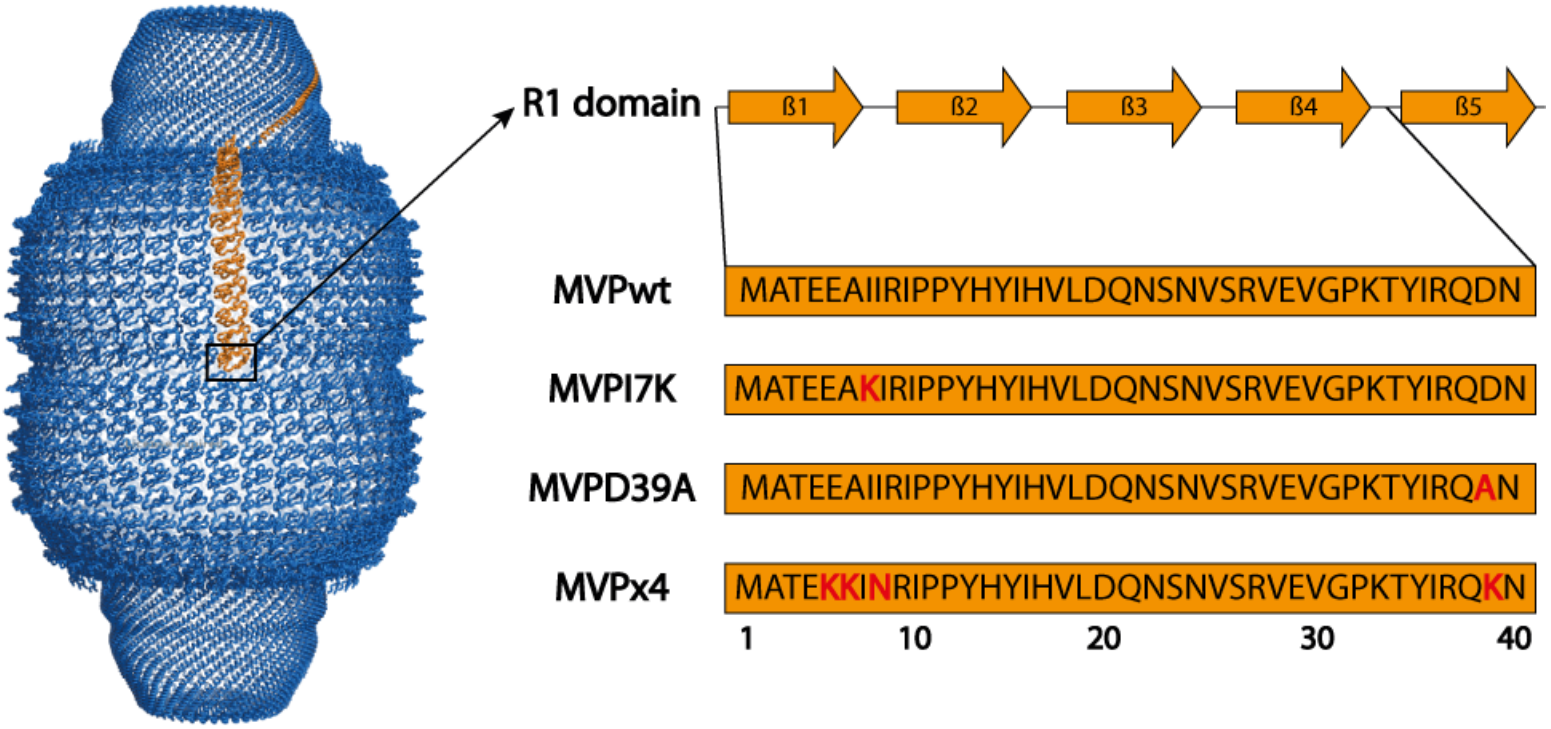
R1 domain
ß1
ß2
ß3
ß4
ß5
MVPwt
MATEEAIIRIPPYHYIHVLDQNSNVSRVEVGPKTYIRQDN
MVPI7K
MATEEAKIRIPPYHYIHVLDQNSNVSRVEVGPKTYIRQDN
MVPD39A
MATEEAIIRIPPYHYIHVLDQNSNVSRVEVGPKTYIRQAN
MVPx4
MATEKKINRIPPYHYIHVLDQNSNVSRVEVGPKTYIRQKN
1
10
20
30
40

Figure S4. MVP R1 mutants generated by recombinant techniques. Left, overall diagram of the vault shell on a ribbon representation. One MVP molecule is depicted orange with the rest are in blue (PDB id: 4HL8). Right, schematic showing the secondary structure the MVP R1 domain. Bottom, in red residues mutated.

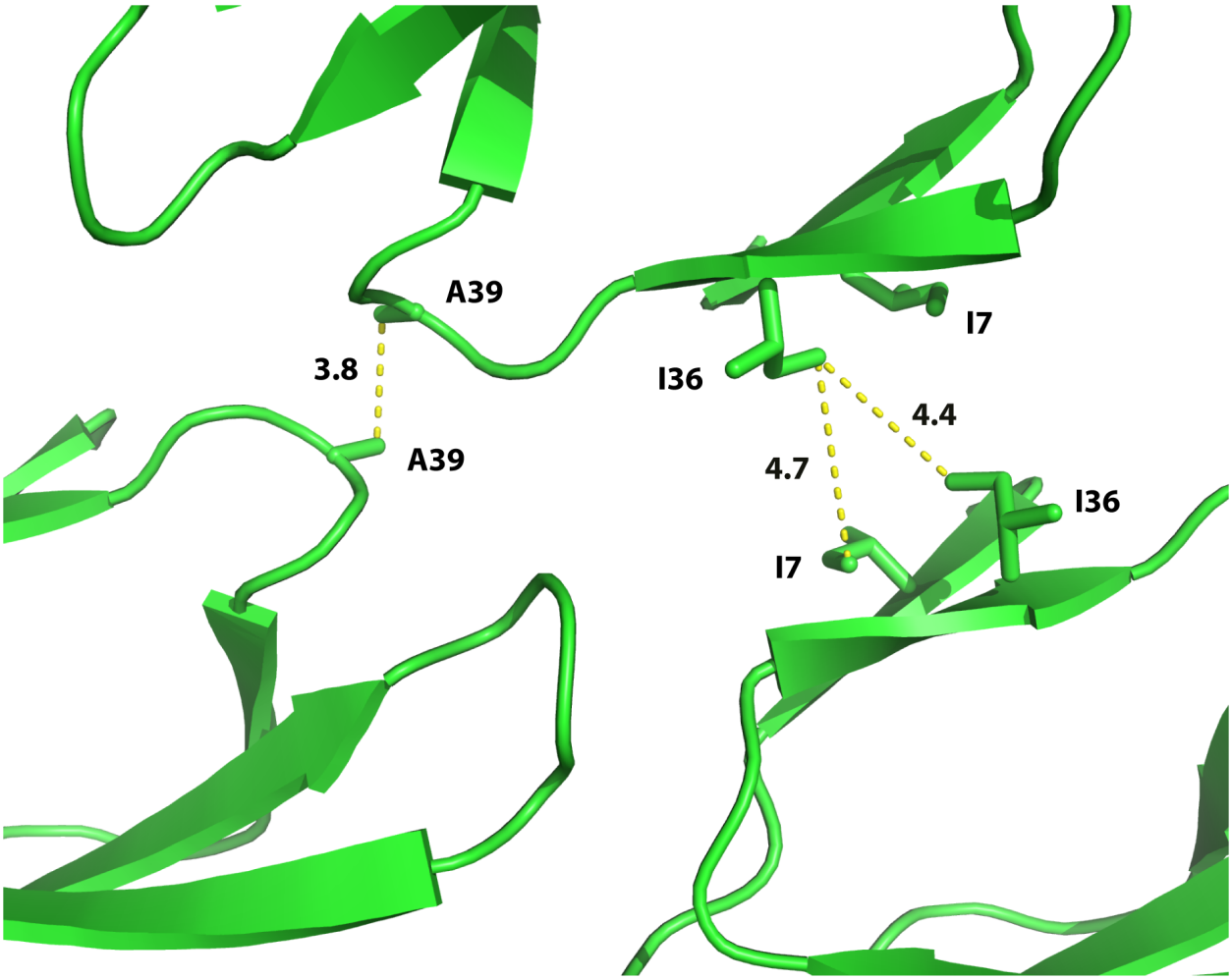
A39
3.8
A39
I7
I36
4.4
4.7
I36
I7

Figure S5. **Model of interactions stablished at the vault midsection in the MVP A39 mutant based on the X-ray structure of MVP (PDB id: 4HL8).** The D39-A substitution was modeled, using Coot *(31)*. Dashed lines in yellow indicate the closest carbon-carbon distances, involving the hydrophobic cluster and the A39 Cβ-Cβ contact. Side chains of residues participating in interactions and shown as sticks and labeled. Contact distances are also explicitly labeled.

A

Vault waist (R1 wt)

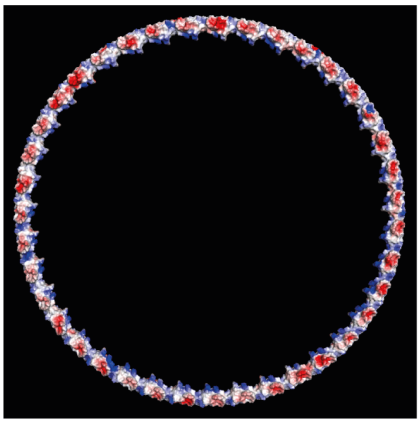

Vault waist (R1 wt)

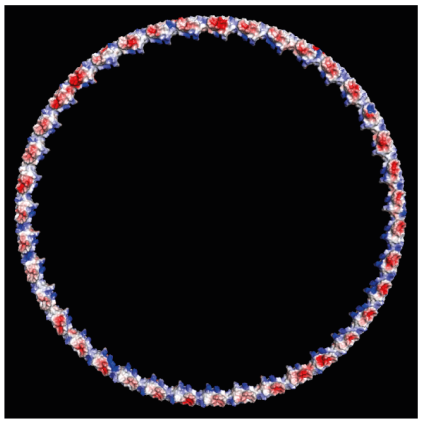

Half vault/half vault interactions mediated by the R1 domains

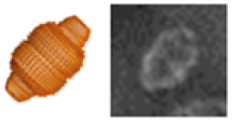

B

Vault waist (R1 MVPx4)

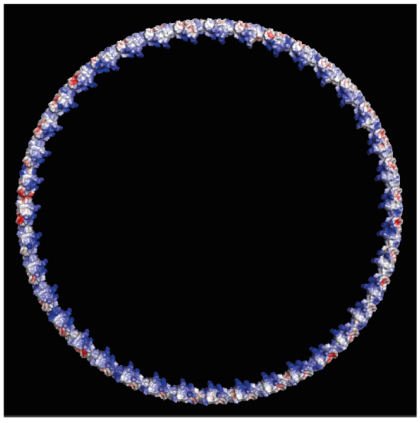

Cap helix and shoulder

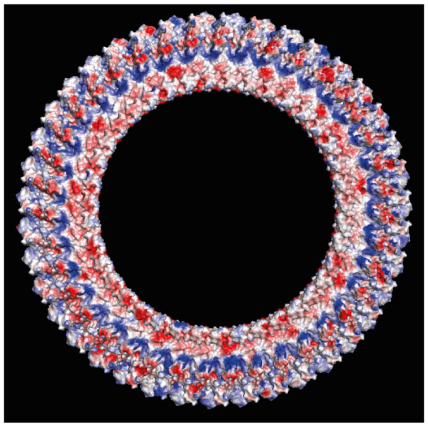

Interactions between vault waist and cap-shoulder domains

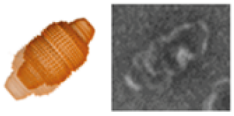

Figure S6. Alternative model for half vault/half vault arrangement in the quadruple MVP (D39K/I7N/E4K/E5K) mutant. (A) The left and central panels show the columbic surfaces of the vault waist as found in the closed wild-type vault structure (PDB id: 4HL8), only R1 domains are displayed. Columbic surfaces were calculated using PyMOL (The PyMOL Molecular Graphics System, Version 2.0 Schrödinger, LLC.). (B) The left panel shows the columbic surface of the vault waist (R1 domains) in a putative R1 model, mimicking the MVPx4 mutant. The D39K/I7N/E4K/E5K substitutions were modeled, using Coot *(31)*. The central panel shows the coulombic surface of the putative interacting region: the base of the cap-helix and shoulder domain has also been calculated (only the first 50 residues that form the base the cap-helix are shown). The charge complementarity between the vault waist and the cap-helix and shoulder regions would favor the presence of vault filaments, formed by an entire vault particle capped with 1, 2 or even 3 vault halves clustered on top of each other. The right panel insets in A and B show individual vaults (A) and vault filaments (B) extracted from micrographs of Figure 3, and the corresponding diagrams assisting on the identification of the views seen on the micrographs.

Table S1. Effect of amino acid substitutions on the distribution of half and entire vaults measured by AFM and EM. Vault populations are showed in %.

	AFM			EM		
	Half solution	Entire	Half filaments	Half solution	Entire	Half filaments
WT	34	66	-	2	98	-
D39A	31	69	-	2	98	-
I7K	43	57	-	12	88	-
MVPx4	94	6	-	5	30	65

Differences in the imaging conditions between EM and AFM techniques result in different vault populations when both techniques are compared. In negative staining TEM the sample is deposited over a C-amorphous film and, after an incubation, is blotted, working in dehydrated conditions. In contrast, in AFM the sample is adsorbed on HOPG surface and remains hydrated during all the experiment. Half vaults imaged by AFM present a massive tendency to be captured on HOPG through the waist *(18, 20),* while TEM images present half-vaults at any orientation (**Figure. S1A**). Taking into account these considerations, the effect of each mutation on the distribution of half vaults and entire vault is in accordance in both techniques. The population of half-vaults increase in the case of I7K and MVPx4 mutant compared to the wildtype and remains similar for the D39A mutant in both techniques.

Table S2. Primers used for the production of the MVP mutants

MVP D39A	
Forward D39A	ACCTACATCCGGCAGGCCAATGAGAGGGTACT
Reverse D39A	CTCTCATTGGCCTGCCGGATGTAGGTCTTTGGT
MVP I7K	
Forward I7K	CAACTGAAGAGGCCAAGATCCGCATC
Reverse I7K	GGGATGCGGATCTTGGCCTCTTCA
MVP X4	
Forward E4/5K	CCATGGCAACTAAAAAGGCCAACATCCGCATC
Reverse E4/5K	GATGCGGATGTTGGCCTTTTTAGTTGCCATGG
Forward I7N	CAACTGAAGAGGCCAACATCCGCATC
Reverse I7N	GGGATGCGGATGTTGGCCTCTTCAG
Forward D39K	GACCTACATCCGGCAGAAGAATGAGAGGGTAC
Reverse D39K	CAAACAGTACCCTCTCATTCTTCTGCCGGATG